Available online at www.sciencedirect.com
ScienceDirect
Journal of Power Sources 173 (2007) 110–120
JOURNAL OF POWER SOURCES
www.elsevier.com/locate/jpowsour

Metamorphosis of the mixed phase PtRu anode catalyst for direct methanol fuel cells after exposure of methanol: In situ and ex situ characterizations

Debasish Chakraborty [a,b,*,1], Ib Chorkendorff [a,c], Tue Johannessen [b,1]

[a] *Center for Individual Nanoparticle Functionality (CINF), Technical University of Denmark, DK-2800 Kgs. Lyngby, Denmark*
[b] *Aerosol Laboratory, Nano.DTU, Department of Chemical Engineering, Technical University of Denmark, DK-2800 Kgs. Lyngby, Denmark*
[c] *Department of Physics, Technical University of Denmark, DK-2800 Kgs. Lyngby, Denmark*

Received 16 January 2007; received in revised form 9 April 2007; accepted 29 April 2007
Available online 5 May 2007

Abstract

The change in the mixed phase heavily oxidized PtRu anode with the exposure of methanol in a direct methanol fuel cell (DMFC) has been investigated by electrochemical impedance spectroscopy (EIS) and X-ray diffraction (XRD). The investigation had two major objectives: (i) to explore the original state of the active catalyst and (ii) to understand if alloying of Pt and Ru is a requirement for higher methanol oxidation activity. It was found that the methanol oxidation activity gradually improved for ∼2 h of exposure. The impedance spectra were taken at different times within this time of improvement of activity. The impedance spectra were deconvoluted in different contributions like membrane resistance (R_m), charge transfer resistance (R_{Ct}), adsorption resistance (R_{ad}), and oxidation resistance (R_{ox}). The improvement of the activity was explained in terms of the effect of the pretreatment on different contributions. XRD was done on the virgin and methanol exposed sample as a possible mean to identify the difference. It was postulated that the reduction of the as prepared PtRu after exposure was responsible for the activity improvement. Also, it was shown that bulk alloy formation is not a necessary condition for higher methanol activity of PtRu catalysts.

Keywords: DMFC; PtRu; Mixed phase; Electrochemical impedance spectroscopy; Time constant; XRD

1. Introduction

The DMFC uses methanol as fuel and has significant advantages over hydrogen-fed proton exchange membrane (PEM) fuel cells in mobile applications in terms of fuel storage and supply [1]. However, one of the main challenges of making DMFC commercially feasible is to improve the slow reaction kinetics of the methanol oxidation reaction at the anode. There is an initial activation overpotential between 0.2 and 0.55 V, depending on the catalyst and operating conditions, required to oxidize methanol anodically at an appreciable rate. At least some of this overpotential is kinetic in nature and could be reduced by suitable catalysts at the anode [2]. Another critical issue of DMFC is the thickness of the anode catalyst layer. A thick catalyst layer increases the ohmic resistance as well as mass transfer resistance for methanol. Therefore to improve the DMFC anode performance it is necessary to investigate on new catalytic materials for methanol electroxidation as well as alternative methods for catalyst preparation and membrane electrode assembly (MEA) fabrication.

Recently we have reported a novel method for one-step electrode preparation by using flame spray pyrolysis (FSP) [3]. The as prepared nanocomposites are a mixture of fcc, mostly unalloyed Pt crystalline phase and an amorphous surface layer, postulated to be a mixture of Pt and Ru oxides. Comparison with commercially available 10% Pt–Ru/C E-TEK catalyst demonstrated that even though the onset potential for methanol oxidation at 90 °C on both catalysts are similar (∼250 mV), the flame prepared Pt1Ru1 has 60% higher activity at 0.4 V. The supported Pt–Ru catalyst has been chosen for comparison because we wanted to observe the difference between a well-alloyed metallic Pt–Ru catalyst and the flame-synthesized catalyst. The unsupported Pt–Ru has been reported to have lesser degree of alloying and a significant presence of RuO_2 compared to carbon suppor-

* Corresponding author. Current address: Amminex A/S, DK-2800 Lyngby, Denmark. Tel.: +45 45252053; fax: +45 45882235.
E-mail addresses: dch@amminex.com, dcktdtu@yahoo.com (D. Chakraborty).
[1] Current address: Amminex A/S, DK-2800 Lyngby, Denmark.

0378-7753/$ – see front matter © 2007 Elsevier B.V. All rights reserved.
doi:10.1016/j.jpowsour.2007.04.057

ted Pt–Ru from E-TEK [4]. The result is interesting considering the debate about the role of oxides in PtRu anode catalyst. While an overwhelming majority of the researchers believe that oxides are harmful to catalytic activities (e.g. [5,6]), according to Rolison et al. the presence of Ru oxides enhances the performance of the DMFC anode [7–9]. Not only that, the Rollison group has specifically suggested avoiding the alloying of PtRu to make better catalyst for methanol oxidation [10].

It is well known that both the physical and chemical properties of the anode catalysts change with the exposure of methanol and during operation [11–13]. Therefore, it is not desirable to relate the electrochemical activity with only ex situ characterization results of as-prepared catalyst. The purpose of our study is to figure out the changes occurring in the PtRu mixed phase catalyst after exposure of methanol and to follow this metamorphosis in situ. Methanol electro-oxidation involves several reaction steps with different rates. Since electrochemical impedance spectroscopy (EIS) can identify processes with different time constants, it should be possible to use EIS to distinguish different elementary steps of the reaction [14]. Therefore, EIS can be used as an in situ technique to follow the changes in the catalytic properties by looking at the changes in the elementary reaction steps. These changes in the reaction rates can then be related to the possible modifications happening in the active layer. Furthermore, besides shedding light on the catalytic properties, EIS can also single out contribution due to protonic conductivity of the catalyst layers [15], and membrane [16]; thickness of the catalyst layer [17], etc. as these properties also change with exposure and conditioning [13,18] when a membrane electrode assembly (MEA) is used in the analysis. Studies in a 'real world electrode environment' is important not only to have a clearer understanding of the reaction at the three phase region, but also to avoid artifacts arising from anion adsorption which results from the use of electrolyte like H_2SO_4 which contains mobile anions [19]. Jiang and Kucernak have reported that the discharge of methanol on Pt is shifted to more negative potentials when Nafion is used as electrolyte instead of H_2SO_4. They attributed the phenomenon to the absence of mobile anions in Nafion [20]. Moreover, it has also been reported that Nafion coating greatly enhances the methanol oxidation activity on Pt [21].

In this work, we used a single cell fuel cell setup with DMFC membrane electrode assembly (MEA) having PtRu nanoparticulate anode synthesized by flame spray pyrolysis. The focus of this paper has been to answer the questions about the state of the mixed phase catalyst after methanol exposure and its effect on the performance. EIS and CV have been used for following the changes in situ and X-ray diffraction (XRD) has been used to characterize the electrodes ex situ before and after the exposures.

2. Experimental

2.1. Electrode preparation

The electrode with Pt to Ru nominal atomic ratio of 1 to 1 (defined as Pt1Ru1) was prepared by using the procedure reported earlier [3,22] with one modification which was to paint the gas diffusion layer, GDL (Toray-090) with a thin layer of VulcanXC72 carbon (CABOT) instead of using bare GDL. The precursors used were ruthenium (III) acetylacetonate ($Ru(acac)_3$, Fluka, purity ≥97%) and platinum (II) acetylacetonate ($Pt(acac)_2$, Aldrich Chemical Co., 97% purity). The solvent was a 4 to 1 volume ratio mixture of isooctane (Fluka, purity 99%) and tetrahydrofuran (Sigma, purity 99%). Forty mg of $Pt(acac)_2$ and $Ru(acac)_3$ each were dissolved in 100 ml of the solvent to make the precursor solution. The solution was pumped by using a syringe pump (IVAC P6000) through a gas-assisted nozzle to spray the precursor solution to the flame zone as small droplets. The nozzle consisted of a capillary tube of outer diameter 0.9 mm (inner diameter 0.6 mm), which is situated in an opening of 1.4 mm diameter creating an annular space of 0.9 mm^2. The design of the nozzle is similar to the one used by Mädler et al. [23]. The precursor solution was passed through the capillary tube at 0.5 mL min^{-1} and oxygen, as both the dispersion and oxidation gas, was introduced through the annulus at 2.2 L min^{-1}. The spray aerosol was ignited by eight hydrogen-fed supporting flames made by horizontal injection through eight equidistant holes drilled in a hollow metal ring placed around the aerosol jet. Cold air, provided from a water-cooled quenching ring was used to quench the aerosol coming out of the flame [24]. The quenching helps decreasing the average particle size by suddenly lowering the temperature and thus decreasing the rate of sintering. The product particles were collected directly on the GDL (Toray TGPH090) by withdrawing the nanoparticle aerosol from the flame through it by using a gas-ejector vacuum pump (PIAB Classic). Here, the Valcun carbon painted GDL was, in principle, applied as a catalyst nanoparticle filter. The thin carbon layer improves the filtration efficiency as well as the performance of the anode in methanol electro-oxidation [25].

2.2. Electrochemical experiments

The flame aerosol produced anodes with a Pt1Ru1 catalyst layer was soaked with 5% Nafion in lower aliphatic alcohol solution (Aldrich Chemical Co.). The ionomer weight was ∼20% of the catalyst. The cathodes (IRD DMFC 3.00) had 1.2 mg cm^{-2} ∼56% Pt/C catalyst (Johnson Matthey) and were obtained courtesy of IRD Fuel Cells A/S. Both the electrodes had a geometric surface area of 3.14 cm^2. The MEA was fabricated by sandwiching Nafion 117 membrane between the anode and the cathode and pressing the assembly at ∼4 bar and 135 °C for 5 min. The cathode, which also acted as a dynamic hydrogen electrode (DHE) [3,5,19], was fed with humidified H_2 at 5 ml min^{-1}. All the experimental results reported in the paper should be taken relative to DHE.

The MEA was loaded inside a single cell fuel cell test station described earlier [3]. Before the introduction of methanol at the anode, the chamber was fed with water for humidifying the membrane and the catalyst layer for 2 h while the cathode was fed with H_2. After 2 h, the cell temperature was raised to 50 °C (or 90 °C) and 1.0 M methanol (99.99%, ACS grade, Sigma–Aldrich) was fed to the anode at 1 ml min^{-1}. After 5 min of the starting of the methanol flow, the following set of measurements was taken: cyclic voltammetry between 0 and 0.8 V

at 5 mV s^{-1}; impedance at open circuit potential; one minute rest (no applied potential); impedance at 0.45 V bias potential. The set was repeated six times with 10 min resting time between each set. Each set, including 10 min resting time, took ∼25 min to complete. After the pretreatments, the anodes were peeled off carefully from the membrane and kept for XRD. The impedance data were taken using single sine option with a sine perturbation of 10 mV rms on top of the bias potential. The cell was allowed a 1 min equilibrium time at the bias potential before starting the measurement. The data were obtained within a frequency range from 100 kHz to 50 mHz with logarithmically spaced 100 data points.

2.3. Physical and chemical characterization

The high-resolution transmission electron microscopy (HRTEM) images and selected area diffraction patterns (SADPs) were taken at the RISOE national laboratory by a JOEL 3000F with an acceleration voltage of 297 kV. The XRD patterns were obtained from the catalyzed GDL with a Philips diffractometer with a Cu K_α radiation source and a nickel filter. The scans were performed over a 2θ range of 20–95° with a scan step of 0.05° and acquisition time of 4s. An external Si standard was used to correct the sample displacement errors [3,26]. The Si powder (Aldrich) was sprinkled carefully on the catalyzed layer before taking XRD pattern.

3. Results and discussion

An overview TEM image of as prepared catalyst is shown in Fig. 1a. The individual catalyst particles range in size from ∼2 to ∼11 nm. While some particles are seen to exist separately, most of the smaller particles form long cluster by neck formation. Patches of darker contrasts can be observed on the crystalline structures. These patches could be amorphous phases of $PtRuO_x$ as discussed in our previous article [3]. The selected area diffraction patterns (SADPs) (Fig. 1b) show diffraction rings of only face-centered cubic (FCC) metallic Pt or very highly Pt rich PtRu alloy. The rings index to: (1) 2.22 Å Pt (1 1 1); (2) 1.98 Å Pt (2 0 0); (3) 1.35 Å Pt (2 2 2); (4) 1.2 Å Pt (3 1 1). Stroud et al. while reporting SADPs of Johnson Matthey PtRu (50 at.

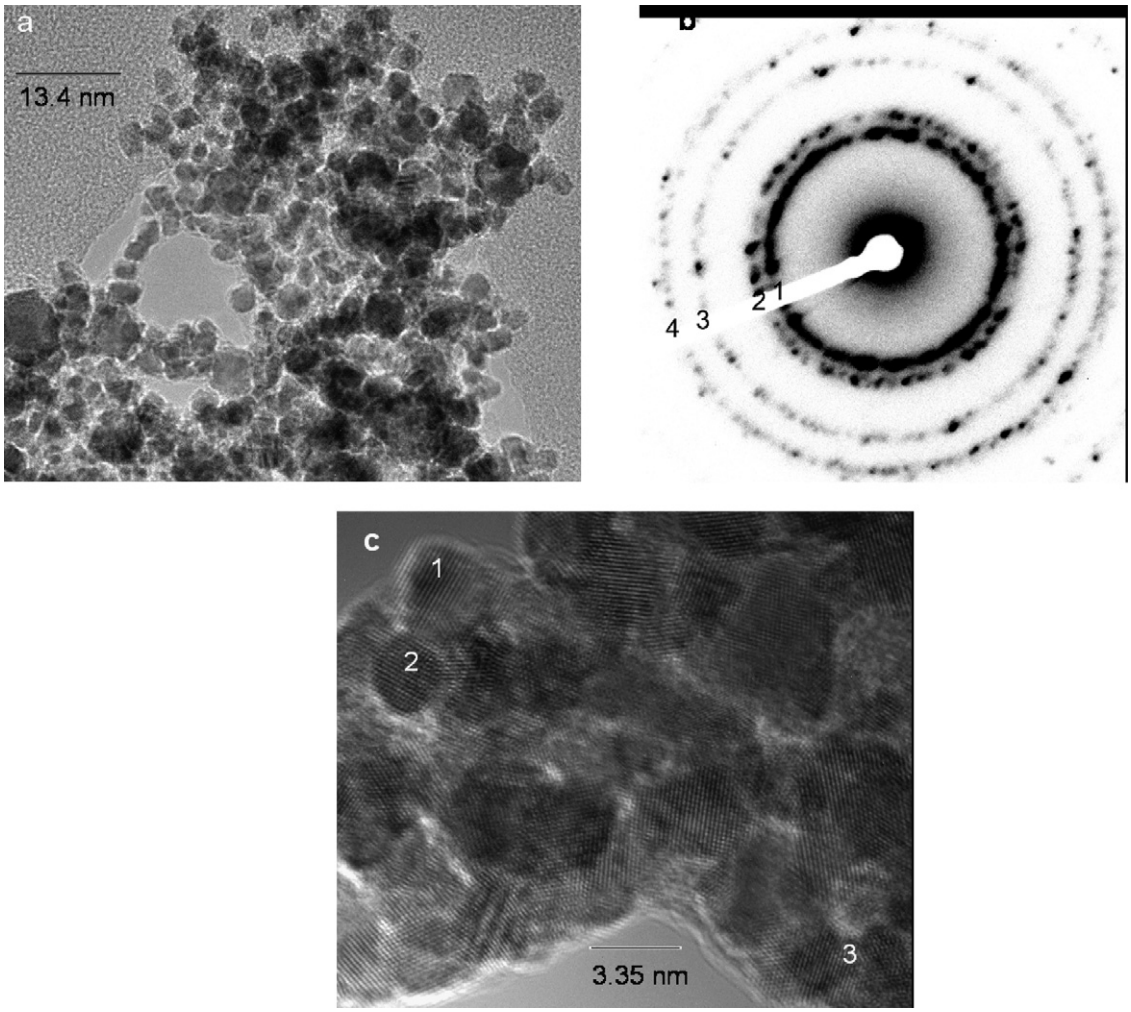

Fig. 1. (a) TEM image showing an overall view of as-prepared PtRu; (b) selected area diffraction patterns of as-prepared PtRu. The sample indexes to metallic Pt: (1) 2.22 Å Pt (1 1 1), (2) 2 Å Pt (2 0 0), (3) 1.35 Å Pt (2 2 0), (4) 1.2 Å Pt (3 1 1); (c) Lattice images of as-prepared PtRu. Pt (1 1 1) denoted by 1, Pt (2 0 0) denoted by 2 and rutile RuO_2 (2 1 1) denoted by three faces are observed. All the unmarked faces in the image are Pt (2 0 0).

%) related the fringes with spacing like (1) with both rutile mixture of (Pt, Ru)O_2 (2 0 0) and fcc metallic PtRu (1 1 1) [27]. But they also observed fringes of rutile (Pt, Ru)O_2 (1 1 0), rutile (Pt, Ru)O_2 (1 0 1), and rutile (Pt, Ru)O_2 (2 1 1), none of which has been observed for our flame made PtRu. Therefore, the fringes producing the first ring can be attributed to Pt (1 1 1) only. No ring indexing to crystalline Ru or any oxide phase is detected. The lattice images of the as-prepared sample (Fig. 1c) show only two fringes found in the SADPs of Pt (1 1 1) and Pt (2 0 0). Interestingly, however, unlike the SADPs, fringes of rutile RuO_2 (2 1 1) with spacing of 1.7 Å can also be found. One possible reason for not getting rings of rutile RuO_2 is that this is present in negligible amount. The TEM images and SADPs nicely complement the conclusion drawn in our previous article [3] about the morphology and composition of the deposit based on XRD, X-ray energy dispersive spectroscopy (EDS) and X-ray photoelectron spectroscopy (XPS). Additionally, possible traces of amorphous materials on the images of the crystalline phases and traces of lattice fringes representing rutile RuO_2 have been observed in the TEM images. To summarize, the flame synthesized PtRu (50 at.%) consists of crystalline phases of metallic Pt or highly Pt rich PtRu alloys and Ru rich amorphous phases of $PtRuO_x$, at least some of which stay in close contact with the crystalline phases. Besides in the amorphous phase, a small amount of Ru may also be present as rutile RuO_2.

Fig. 2a shows the improvement in polarization behavior with time as the PtRu catalyst was exposed to methanol. After 100 min of exposure of methanol at 50 °C, the improvement plateaus to a value ~20 from ~7.5 mA cm^{-2} at the beginning. Fig. 2b shows the change in current density with time at 0.45 V read from the CVs for the 50 °C (Fig. 2a) and the 90 °C exposures (not shown). The interesting point to note from these figures is that the rate of change of current density varies for two temperatures. After 30 min, the rates of current density change are 0.17 and 0.94 mA cm^{-2} min^{-1} for 50 and 90 °C, respectively. The rates of change, after 60 min have become 0.1 and 0.2 mA cm^{-2} min^{-1} for 50 and 90 °C, respectively. At 50 °C, going from 30 to 60 min, the rate decreases by only 0.07 mA cm^{-2} min^{-1}. On the contrary, at 90 °C, going from 30 to 60 min, the rate decreases by 0.74 mA cm^{-2} min^{-1}. This means that at higher temperature the process reaches towards equilibrium much faster or in other words the process is kinetically controlled.

The impedance spectra taken at different times during conditioning are shown in Fig. 3. It could be seen that the *x*-axis intercept of the capacitive loop decreases with time of exposure at 50 °C from ~19 to ~11 Ω cm^2. The spectra show pseudoinductive behavior at low frequencies, which is very typical of reactions with adsorbed intermediates [28,29]. In a recent article, it has been shown that the occurrence of pseudoinductive loop and onset potential coincide for methanol oxidation on PtRu. It has also been observed that the occurrence of the pseudoinductive loop lowers the *x*-axis intercept of the spectra [14]. A very similar scenario arises in case of the anodic dissolution of Mg in chloride and sulphate solutions. It has been proposed based on Cao's theory that the inductive loop could be attributed mainly to the broken area of the protective surface film and the capacitive loop is related to the Mg^+ concentration within the broken

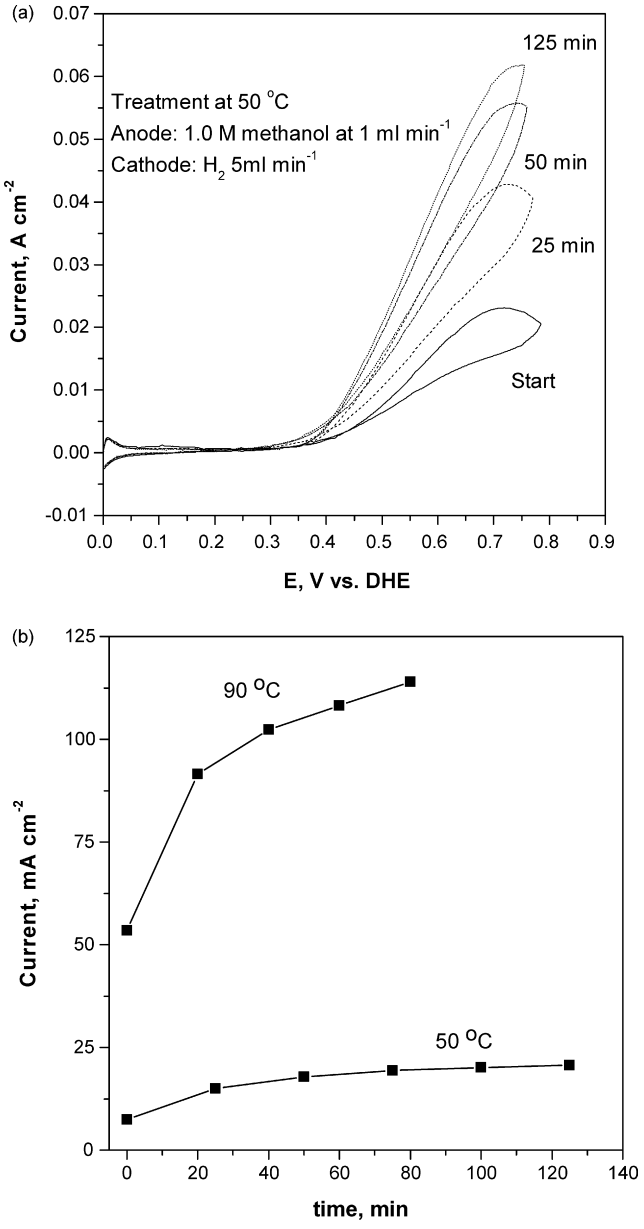

Fig. 2. (a) Improvement of methanol oxidation activity with pretreatment. The CVs are (i) 0 min, (ii) 25 min, (iii) 50 min and (iv) 125 min at 50 °C; (b) change in current density with pretreatment at 0.45 V read from CV. Lines in b are for guiding the eye and not the result of any curve fitting. Anode: flame prepared PtRu ~0.28 mg cm^{-2} and cathode: 1.2 mg cm^{-2} ~56% Pt/C (Johnson Matthey).

area [30]. Interestingly, methanol oxidation on PtRu can also be explained using the same analogy as Mg dissolution. Before the onset, the catalysts surface is completely covered by the adsorbed hydrogen and residues from methanol dehydrogenation. So, there is no free site (like broken protective layer for Mg dissolution) available for further methanol oxidation. When the potential goes to the onset (and above), holes are created in the adsorbed layer by the oxidation of the residues. So, we observed the inductive loop only after the onset potential. Therefore, we could relate the capacitive loop to the concentration of the residues in the holes. However, to get quantitative information from the spectra, fitting of the data with a suitable equivalent circuit

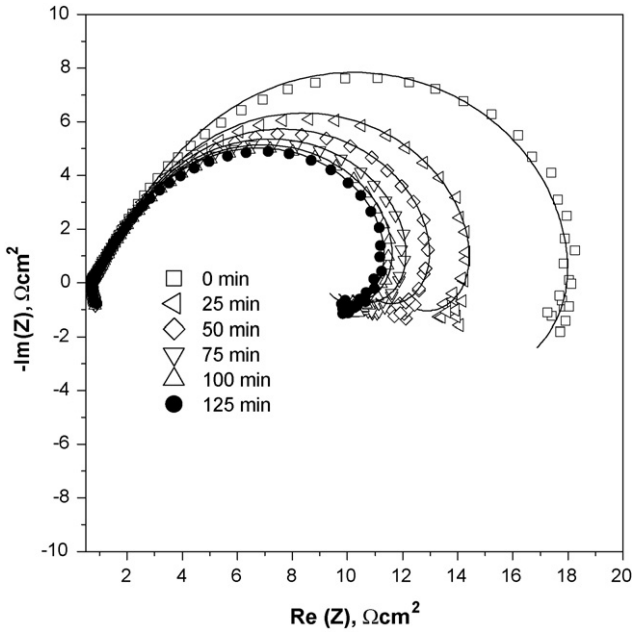

Fig. 3. Nyquist plots showing the improvement of the anode performance. Points: experiments data; lines: obtained by fitting the data to equivalent circuit shown in Fig. 4. Anode: flame prepared PtRu ~0.28 mg cm^{-2} and cathode: 1.2 mg cm^{-2} ~56% Pt/C (Johnson Matthey).

is necessary. The circuit shown in Fig. 4 was found suitable to fit the data. The methanol electrooxidation reaction on PtRu can be defined in general by the following steps:

$$(CH_3OH)_{sol} \rightarrow (CH_3OH)_{ads} \rightarrow CO_{ads} + 4H^+ + 4e^- \quad (1)$$

$$H_2O \rightarrow (OH)_{ads} + H^+ + e^- \quad (2)$$

$$(CO)_{ads} + (OH)_{ads} \rightarrow CO_2 + H^+ + e^- \quad (3)$$

The above reaction scheme is the generally accepted methanol electrooxidation reaction mechanism on PtRu [31–36], even though the existence of other parallel pathways had also been suggested [37]. The methanol dehydrogenation reaction (Eq. (1)) is a multi-step process producing one or more surface bound species. However, only $(CO)_{ads}$ species has been detected by spectroscopic studies, implying that the other surface bound intermediates have very short lifetime to be detected. Second step (Eq. (2)) and the final step (Eq. (3)) are the water activation and residue oxidation step, respectively. By considering the above-mentioned mechanism, we may assign different elements of Fig. 4 to the possible reaction equivalents. The resistance R_{Ct} can be assigned to the charge transfer process. The $(C_{ad}R_{ad})$ analog can be assigned to the adsorption and dehydrogenation

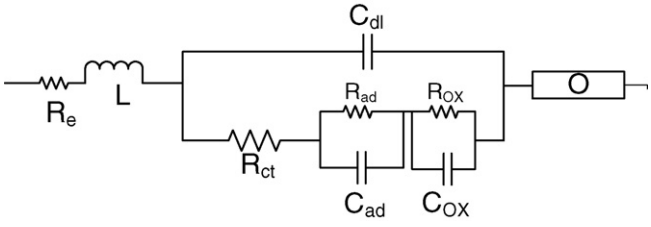

Fig. 4. Equivalent circuit used for fitting impedance data.

process. Both R_{ox} and C_{ox} have negative values because the $(C_{ox}R_{ox})$ analog represents the inductive loop. The $(C_{ox}R_{ox})$ analog can be assigned to the surface bound residue oxidation process. This assignment can be rationalized by the effect of R_{ox} on the whole circuit. Because it has a negative value, it decreases the total cell resistance. The same effect can be expected if the surface bound residues are oxidized to make free sites available for the methanol oxidation reaction to proceed. The capacitance C_{dl}, placed in parallel with the $R_{Ct}(C_{ad}R_{ad})(C_{ox}R_{ox})$, accounts for the effect of the double layer. The resistance, R_e and the inductance, L, outside the double layer capacitance are due to the electrolyte (membrane) resistance and the effect of connecting wires and metals plates, respectively. The element O, known as the finite length diffusion Warburg element has the following expression for impedance:

$$Z_O = \tanh \frac{B\sqrt{j\omega}}{Y_0(\sqrt{j\omega})} \quad (4)$$

where ω is the frequency and B and Y_0 are fitted parameters defined as

$$Y_0 = \frac{n^2F^2Ac(D)^{0.5}}{RT} \quad (5)$$

$$B = \frac{\delta}{D^{0.5}} \quad (6)$$

where δ is the thickness of the diffusion layer (cm), A the real surface area of the working electrode (cm^2), D the diffusion constant of the species concerned (cm^2 s^{-1}), n the number of electrons transferred, F the Faraday constant (C mol^{-1}), and c is the concentration in the bulk (mol cm^{-3}). The fitted parameter B is the square root of the diffusion time constant τ_D [38]. The position of the finite length diffusion element outside the double layer analog represents a diffusion process that is not rate determining for the system [39].

Fig. 5 shows the different fitted parameters. Fig. 5a shows that Y_0 is increasing while B is decreasing with time of pretreatment. According to Eqs. (5) and (6), the trends of Y_0 and B indicates that the diffusion process is improving with the pretreatment. However, the maximum value of the diffusion time constant, τ_D, is ~0.044 s. This time constant is at least an order of magnitude lower than the time constant of the rate-determining step (discussed in the subsequent paragraphs). Therefore, the diffusion process will have no influence what so ever on the overall kinetics. It can be seen from Fig. 5b that the value of the membrane resistance, R_e (~0.71 Ω cm^2) does not vary appreciably with the duration of pretreatment. Therefore, it does not have any significant influence on the performance improvement. Moreover, the polarization curves are corrected for iR losses using these values of R_e, taking out the contribution of these resistances. The pretreatment also does not significantly change the value of C_{dl}, which remains ~4 mF cm^{-2} (Fig. 5c). It has been suggested that the electrochemically active surface areas may be estimated by the values of C_{dl} which is usually proportional to the active surface area [18,40–44]. This method can be especially very useful for unsupported catalyst [44]. If that is really the case, it can be deduced from the of C_{dl} values that the three phase area or elec-

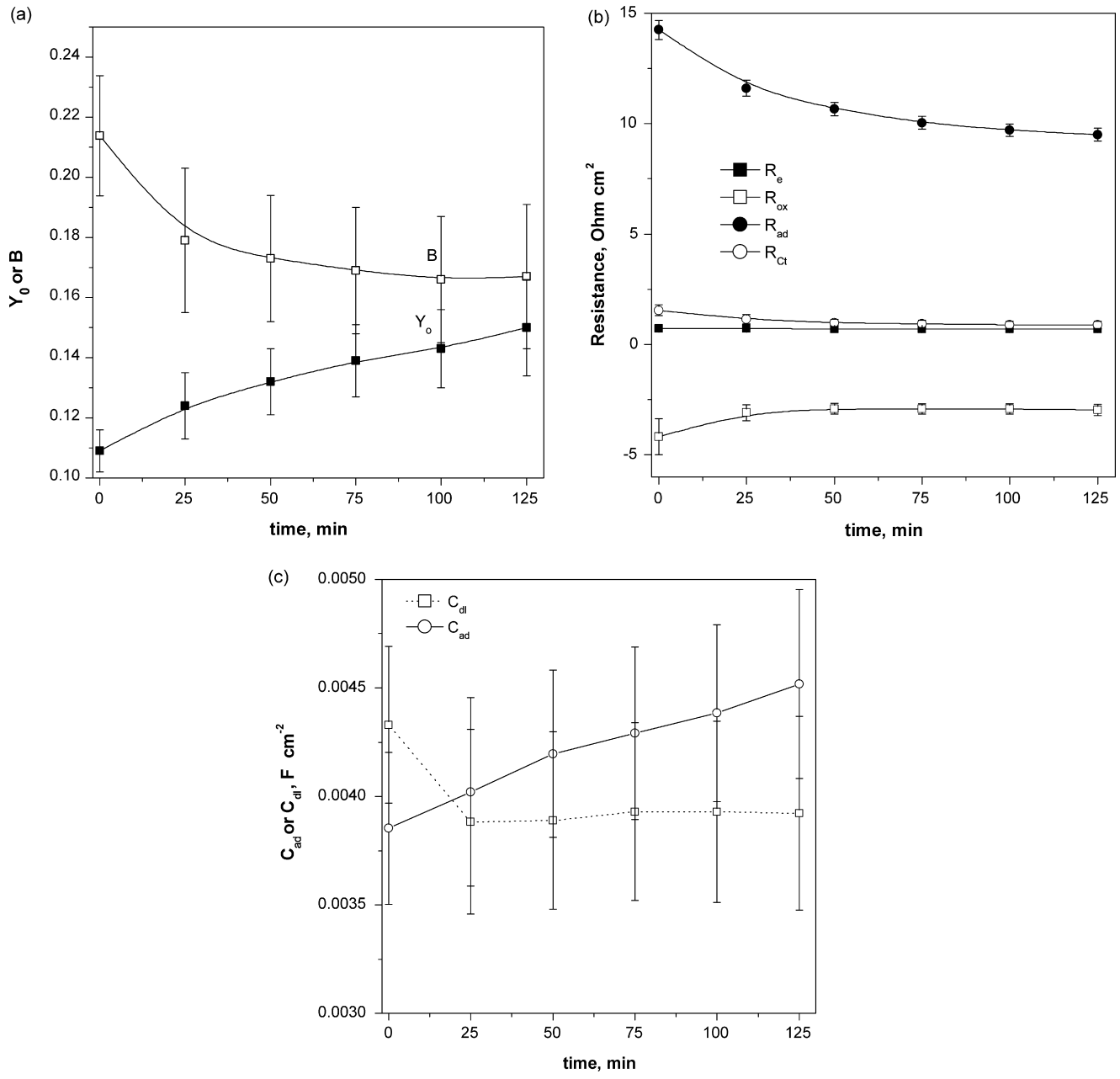

Fig. 5. Variation of different parameters of the equivalent circuit with time. (a) Y_0, B vs. time; (b) resistances vs. time; (c) pseudocapacitances vs. time. The inductance L remains unchanged at $\sim 1.4 \times 10^{-6}$ H cm^2. Anode: flame prepared PtRu $\sim$0.28 mg cm^{-2} and cathode: 1.2 mg cm^{-2} $\sim$56% Pt/C (Johnson Matthey).

troactive surface area of the anode catalyst layer remains more or less unchanged with pretreatment.

Fig. 5b shows that even though R_{Ct}, R_{ad}, and R_{ox} are changing with time of pretreatment, the major contributions to the cell resistance come from R_{ad} and R_{ox}. The charge transfer resistance, R_{Ct}, decreases from a value of $\sim$1.4 Ω cm^2 at the beginning to a value of $\sim$0.9 Ω cm^2 after the pretreatment has been completed. The adsorption resistance, R_{ad}, however, shows a decrease from 14.25 Ω cm^2 at the beginning to 9.5 Ω cm^2 after 125 min. The meaning of this decrease from kinetics point of view is that the resistance for the adsorption of methanol is decreasing with pretreatment. The adsorption pseudocapacitance, C_{ad}, increases from 0.00385 to 0.00452 F cm^{-2} after 125 min (Fig. 5c). One interpretation of this increase is that the adsorption isotherm is becoming steeper with pretreatment. However, the time constant for the adsorption and dehydrogenation process ($\tau_{ad} = R_{ad}C_{ad}$) decreases, albeit slightly, with the time of pretreatment meaning that the kinetics of the process represented by τ_{ad} is improving with pretreatment (Fig. 6). The oxidation resistance, R_{ox}, which is beneficial to the cell performance, on the other hand, shows a steady gradual decrease in value from $\sim$4.2 to $\sim$3 Ω cm^2 after 125 min (Fig. 5b). The value of the oxidation pseudocapacitance also decreases with the pretreatment time from $\sim$0.54 to $\sim$0.23 F cm^{-2}. The time constant of the oxidation process ($\tau_{ox} = R_{ox}C_{ox}$) also shows a gradual decrease with pretreatment (Fig. 6).

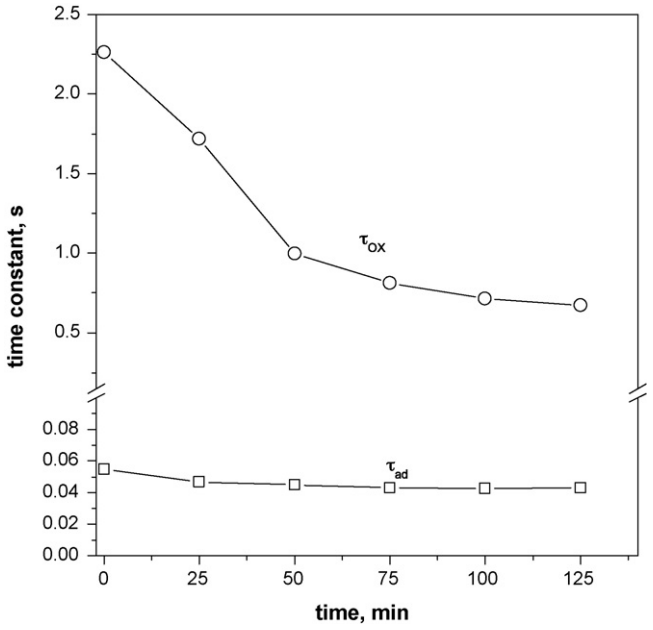

Fig. 6. Variation of time constant with pre-treatment; τ_{ad}: adsorption and dehydrogenation time constant and τ_{ox}: oxidation time constant. The lines are guide to the eye and not the result of curve fitting.

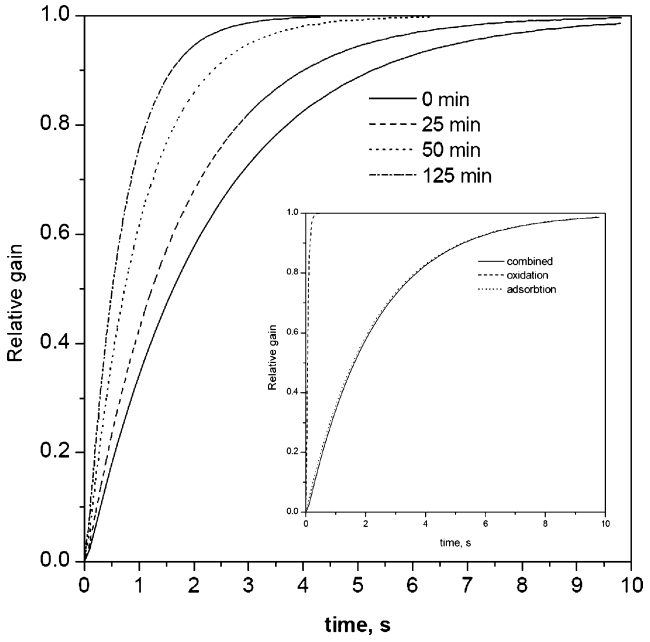

Fig. 7. Response of the system for a step change in potential at different times. Insert: relation between the overall process and the oxidation and adsorption process simulated by using the data of 0 min response.

The effect of changing time constants on the whole process can be explored by using a transfer function approach. We shall assume that the process of adsorption and oxidation are non-interacting, i.e. the adsorption process affects the residue oxidation process but the former is not significantly affected by the later. This assumption is indeed valid because the τ_{ox} is at least an order of magnitude higher than τ_{ad}. Kinetically, this means that one can expect a complete coverage of the residues whatever the oxidation rate is. The consideration of non-interaction gives a combined transfer function of the adsorption and oxidation process as follows [45]:

$$G(s) = \frac{K_a}{\tau_{ad}s + 1}\frac{K_o}{\tau_{ox}s + 1} \tag{7}$$

where K_a and K_o are gains of the adsorption and oxidation processes. The current response of the two non-interacting systems to a unit step change in the potential is given by [45]

$$i(t) = K\left[1 + \frac{1}{\tau_{ox} - \tau_{ad}}\left(\tau_{ad}\exp\left(\frac{-t}{\tau_{ad}}\right) - \tau_{ox}\exp\left(\frac{-t}{\tau_{ox}}\right)\right)\right] \tag{8}$$

Fig. 7 shows the response of the system for a step change in potential at different times. It is clearly seen that the time to reach a steady state after a step change in potential decreases as the pretreatment time increases. At the start the time is around 10 s whereas after 125 min, it becomes around 2.5 s. As shown by the insert of Fig. 7, the decrease is closely related to the decrease in τ_{ox}. This is in compliance with the assumption that oxidation of surface residue is the rate limiting step. Now the question is whether these improvement be explained based on the chemistry of PtRu after the catalyst being exposed to methanol in a fuel cell.

Bulk Pt and Ru oxides, as discussed by Holstein and Rosenfeld based on the compilations of Pourbaix (at pH 0, hydrogen partial pressure = 1 atm), are not thermodynamically stable below ~0.8 V versus RHE even in the absence of reducing molecules like methanol [46]. Because of the acidic Nafion in a wet cell, the pH of the anode should be fairly close to zero. Moreover, the presence of methanol could only make the reducing condition stronger. The reduction of Pt and Ru oxides, present in the as prepared PtRu catalyst, to metallic states after being used as DMFC anode has been reported by O'Grady et al. [11]. They also observed by means of in situ X-ray adsorption spectroscopy (XAS) that both Pt and Ru oxides are completely reduced to metallic form even when the catalyst was held at 0.1 V versus RHE in 0.1 M H_2SO_4. Viswanathan et al. have reported similar reduction of both Pt and Ru oxides during fuel cell operation with reformate-air [12]. Based on the above discussion, a plausible mechanism of the reduction of the anode catalyst in presence of methanol can be proposed as follows:

$$PtO_x + H^+ \Leftrightarrow Pt + H_2O \tag{9}$$

$$Pt + H^+ + e^- \Leftrightarrow Pt - H \tag{10}$$

$$2Pt + CH_3OH \rightarrow Pt - COH_x + P - H \tag{11}$$

$$Pt - COH_x + Pt - O_x \rightarrow 2Pt + CO_2 + H_2O \tag{12}$$

$$Pt - COH_x + RuO_x \rightarrow Pt + Ru + CO_2 + H_2O \tag{13}$$

$$Pt - H + PtO_x \rightarrow 2Pt + H_2O \tag{14}$$

$$Pt - H + RuO_x \rightarrow Pt + Ru + H_2O \tag{15}$$

As mentioned before, the picture that emerges from the various characterization of the as-prepared catalyst is an amor-

phous skin consisting of a mixture of PtO_x and RuO_x on top of a crystalline mostly unalloyed Pt core. When this amorphous phase becomes exposed to a pH very close to zero which is the most likely situation in the catalyst layer of a DMFC, some PtO_x will reduce first to form metallic Pt because it is thermodynamically unstable (Eq. (9)). Even though, RuO_x is also thermodynamically unstable at near zero pH, PtO_x will probably be reduced to Pt faster because Pt is nobler than Ru. Now the Pt will adsorb and dehydrogenate methanol to from Pt–COH_x and Pt–H. These two species will further reduce both neighboring PtO_x and RuO_x to create metallic Pt and Ru (Eqs. (12)–(15)). It should be mentioned that the process of reduction could also be possible without methanol through Eqs. (9), (10), (14) and (15). It has been deduced by Davies et al. that both H_2 and CO could reduce oxidized PtRu even at room temperature and contrary to thermodynamic predictions, H_2 is a more efficient reducing agent of PtRu oxides compared to CO [47]. The presence of methanol will improve the kinetics of the reduction process by not only supplying carbon containing residues (COH_x), but also providing higher concentration of Pt–H produced from the dehydrogenation of methanol. Therefore, it is most likely that as the pretreatment proceeds, we are going to have more and more PtO_x and RuO_x reducing to metallic form.

It is well accepted that PtO_x blocks the initial stage of the methanol oxidation process because it is a C–H bond cleavage process which requires a metal surface site that can stabilize H_{ads} intermediate [5,10]. Therefore it is most likely that with the reduction of PtO_x to metallic Pt, the resistance for adsorption, R_{ad} will decrease. But the step of adsorption of methanol will not have any effect on the improvement of activity as the rate limiting step is the oxidation of the surface bound residues. Therefore, the residue oxidation step must have to improve to show an improvement in the overall performance. The residue oxidation at the low potential (~0.4 V) requires surface oxides on Ru as on Pt surface oxides do not form below 0.5 V versus RHE [20]. However, there is still no consensus yet if the presence of RuO_x or Ru in the anode catalysts is better for the residue oxidation process. Rolison et al. have argued that the presence of RuO_x is beneficial not only because it is an excellent proton conductor but also its ability in hydrous form to supply Ru–OH species required for the bifunctional mechanism according to the following reaction [8,10]:

$$Ru^{+4} - O^{2-} + H^{+} + e \leftrightarrow Ru^{3+} - OH^{-} \quad (16)$$

However, the majority of the researchers have opposed the idea of RuO_x having any beneficial effect in terms of supplying the oxygenated species required for the cleaning of surface residues. On the contrary, it has been postulated that the presence of oxides is detrimental by way of blocking of the active sites [5,6,48]. Moreover, based on thermodynamics and XAS studies, it is hard to conceive that the RuO_x detected in the as prepared PtRu catalysts will be stable enough to remain as oxides under the DMFC operating conditions. We also would like to postulate that the improvement in the performance with pretreatment is related to the reduction of both the PtO_x and RuO_x present in the as prepared catalyst. In order to test the hypothesis, XRD has been done on both the virgin and pretreated anode catalysts.

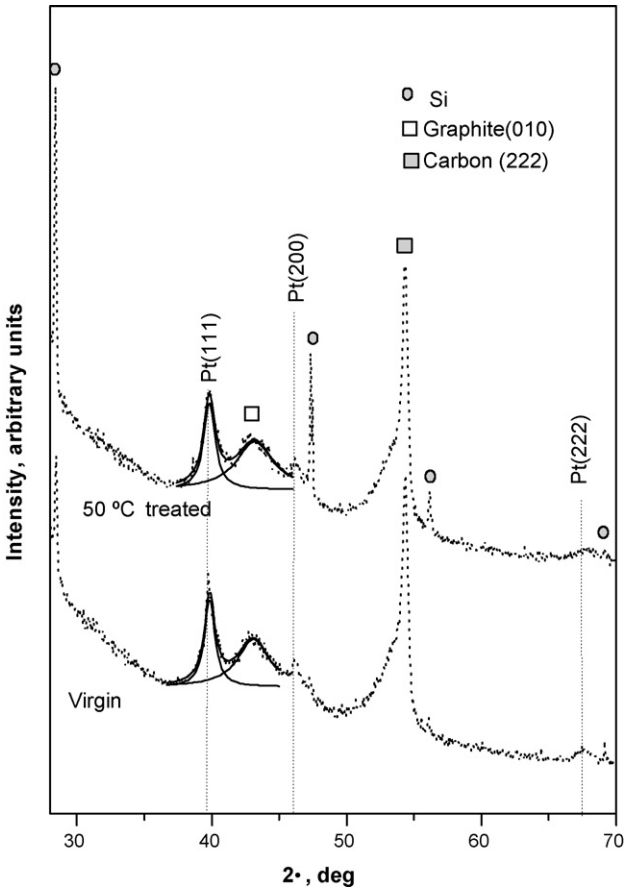

Fig. 8. XRD of the virgin and 50 °C treated anode. Si powder sprinkled on the catalyst layers served as an external standard for correcting sample displacement errors. Besides peaks for Pt face centered cubic (fcc) phase, peaks for Si and C are also observed. The dotted lines are experimental data and the solid lines show the fitted Lorentzian peaks. The spectra were collected between the 2θ values of 20° and 95°; however, a zoomed-in window of 25–70° is shown.

Fig. 8 shows the XRD of the virgin electrode and the pretreated anode. Only deflections from the face centered cubic (fcc) lattices of Pt metal are observed; absent are lines from hexagonal closed-packed (hpc) lattice of Ru metal. This is typical of PtRu containing ≥50 at.% Pt [49–51]. The Pt peaks of the pretreated sample show no shift from the virgin sample. The lattice parameters (a_{fcc}) and the average particle size (d) for the nanocrystalline phase are calculated from the peak positions and peak broadenings, respectively, of Pt (1 1 1) by using the following formula:

$$a_{fcc} = \frac{\sqrt{3}\lambda}{2\sin\theta} \quad (17)$$

$$d = \frac{K\lambda}{\beta\cos\theta} \quad (18)$$

where $\lambda = 1.54056$ Å is the wavelength of radiation used, K a constant (a value of 0.9 is used), θ and β are the Bragg angle and the width of the measured peak, respectively.

Table 1
Fitted parameters of the XRD pattern

Sample	Peak position of fcc phase (°)	Peak width of fcc phase (°)	R^2	Lattice parameter (a_{fcc}) (nm)	Average particle size (nm)	Position of neighboring peak (°)
Virgin	39.84 ± 0.01	0.94 ± 0.03	0.95	3.916 ± 0.001	9.0 ± 0.29	43.08 ± 0.036
50 °C treated	39.82 ± 0.011	1.024 ± 0.04	0.94	3.917 ± 0.001	8.25 ± 0.32	43.18 ± 0.04

The Pt (1 1 1) peaks have been fitted with Lorentzian function considering the interference from the graphite (0 1 0) peaks which have also been fitted with Lorentzian function. The details of the fitting parameter along with the lattice parameters (a_{fcc}) calculated from Eq. (17) and average particle size calculated from Eq. (18) are shown in Table 1. Also included are the positions of the neighboring peak which remains more or less constant at 43.1°, to show the accuracy of the estimate. The position of the diffraction of the fcc crystalline phase remains more or less unchanged for the samples at ∼39.8° which gives an a_{fcc} value of ∼3.92 Å. This lattice parameter implies that the crystalline phase for all the samples are pure Pt. The particle size, however, varies slightly for the two samples: 9 nm for the virgin sample, 8.25 nm for the pretreated sample. Now, we could try to explain the XRD results considering the reduction mechanism proposed above. The mixed oxide amorphous skin gets reduced to form metallic Pt and Ru. Therefore, due to reduction, most likely a mixture of Pt and Ru will be formed. That the newly formed Pt and Ru remain as a haphazard mixture than forming long-range order is evident from the lack of any sign of alloying even after the pretreatment. The slight decrease in the average particle size after the pretreatment may be due to the smaller particles of Pt formed during the pretreatment process. There is no evidence of the hexagonal closed pack (hcp) Ru peak in the XRD after pretreatment possibly either because the Ru particles are two small to produce diffractions which can be separated from the background or as the sample has been exposed to ambient after pretreatment, Ru is phased out as amorphous RuO_x. In fact it has been reported by Viswanathan et al. that the reduction of RuO_x of PtRu during pretreatment is pretty much reversible: the Ru K-edge X-ray adsorption near-edge spectrum of the pretreated but air-exposed sample resembled that of fresh sample [12].

Now we would like to comment on the previously reported [3] higher mass activity of the flame synthesized PtRu mixed phase catalysts compared to the well alloyed 10% PtRu/C (E-TEK) based on the above discussions. In the article it was mentioned that the anode treated with H_2 and methanol at 90 °C for making it stable. The results presented above suggest the exposure of methanol to the flame synthesized mixed phase anode produces a mixture of metallic Pt and Ru with the absence of long-range order. It has been shown that physical mixture of Pt and Ru, Ru decorated Pt, and Pt decorated Ru are as good as or better for methanol as well as H_2/CO oxidation [52–56]. Our results in this work along with our previous paper show that the mixed phase unalloyed PtRu can have better activity for methanol oxidation in a fuel cell compared to well-alloyed PtRu. It seems that for bifunctional mechanism, the most widely proposed mechanism for the promotion of Pt by Ru [7,32,34,35,57], to be active the proximity of the Pt and Ru sites is the most important criterion: the proximity could either be achieved by alloying or the methods mentioned above.

Finally, to show that the undetectable Ru has indeed a role to play in the mixed phase catalyst, the anode has been given severe treatment with different cycles up to 1.6 V versus DHE for more than 30 h. Preferential Ru dissolution from bulk PtRu alloy with 7 at.% Ru was reported by Gasteiger et al. when cycling between 0.075 and 0.95 V versus RHE. Significant change in the electrode behavior was observed even after 10 cycles at 20 mV s^{-1}. However, the PtRu with 46 at.% of Ru was stable after 10 cycles [58]. Davies et al. reported oxidative dissolution of Ru deposited on Pt (1 1 1) and Pt (1 1 0) and concluded that the stability of PtRu against Ru dissolution increases when Ru was incorporated in an alloy on Pt surfaces [59,60]. Behm et al. reported dissolution of Ru from nanoparticulate PtRu after cycling it to a higher potential of 0.8 V versus RHE [61]. Holstein and Rosenfeld by using X-ray absorption spectroscopy (XAS) reported that Ru dissolution occurs in presence of methanol also: nafion mixed 20% 1:1 PtRu/C anode dipped in 1.0 M methanol + 0.5 M H_2SO_4 lost over half of the Ru during the first 12 cycle from 0.01 to 1.36 V versus RHE at 20 mV s^{-1} at 25 °C. The Ru loss was also observed when the experiment was done with the PtRu/C as anode of a DMFC under the same conditions, albeit the loss was slower compared to liquid electrolyte [46]. Compared to the above-mentioned reports, the flame prepared mixed phase PtRu showed remarkable stability. The anode has been cycled

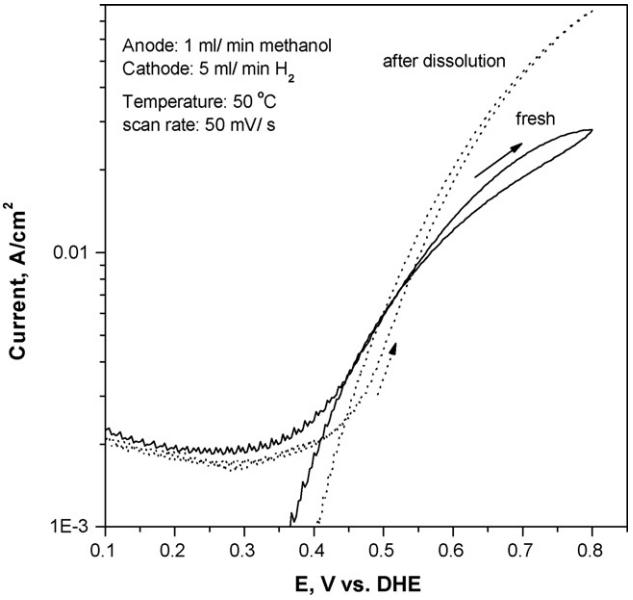

Fig. 9. Plot of log(*I*) vs. *E* for fresh and Ru depleted anode. The potential is not corrected for i*R* loss.

for more than 30 h to demonstrate the effect of Ru dissolution. The effect of Ru dissolution can be observed in Fig. 9. The onset of methanol oxidation moved to ∼45 mV more positive potentials compared to the relatively fresh anode. It can also be seen that below 0.55 V, the fresh anode performs better compared to the Ru depleted anode. However, potential above 0.55 V, the Ru depleted anode shows much better performance. These observations are similar to the reports of methanol oxidation on PtRu with different compositions at room temperature: as the working potential increases, the catalysts containing lower loading of Ru performs better with Pt being the most active at very high but technologically irrelevant applied potentials [62,63]. Even though our experiments have been done at 50 °C, one should not expect to see a change in the above-mentioned trend of room temperature methanol oxidation on PtRu below 60 °C. Only above 60 °C, Ru, besides Pt, starts to adsorb and dissociate methanol and therefore the kinetics can be different from the room temperature kinetics [62]. Therefore, Ru in the mixed phase PtRu catalyst does play a role of lowering the onset potential of methanol oxidation by most probably producing surface oxides at a lower potential than Pt.

4. Conclusion

It has been shown that the activity of the flame synthesized as-prepared mixed phase PtRu anode toward methanol oxidation improves with the exposure of methanol. An improvement in the activity of the catalyst has been observed with a 50 °C treatment for 125 min. The XRD analysis showed that the crystalline phase of the catalyst was unalloyed fcc Pt for both as-prepared and pretreated samples. However, the average particle size changed with exposure of methanol: from ∼9 nm for the virgin catalyst to ∼8.25 nm for 50 °C treated sample. A mechanism of the reconstruction process through the reduction of $PtRuO_x$ skins has been proposed. It was deduced that at the DMFC operating conditions the PtRu anode exists in metallic states. Even though the catalyst remains unalloyed, a close proximity of the Pt and Ru active sites enables the promotion of Pt by Ru.

Acknowledgements

This work was supported by PSO (project 5357). Center for Individual Nanoparticle Functionality (CINF) is sponsored by the Danish National Research Foundation. The authors wish to thank IRD Fuel Cells A/S for the collaboration. Assistance form SGL Carbon is also gratefully acknowledged.

References

[1] B.D. McNicol, D.A.J. Rand, K.R. Williams, J. Power Sources 83 (1999) 15–31.
[2] G.T. Burstein, C.J. Barnett, A.R. Kucernak, K.R. Williams, Catal. Today 38 (1997) 425–437.
[3] D. Chakraborty, H. Bischoff, I. Chorkendorff, T. Johannessen, J. Electrochem. Soc. 152 (2005) A2357–A2363.
[4] A.S. Aricò, A.K. Shukla, K.M. El Khatib, P. Cretì, V. Antonucci, J. Appl. Electrochem. 29 (1999) 671–676.
[5] H.N. Dinh, X. Ren, F.H. Garzon, P. Zelenay, S. Gottesfeld, J. Electroanal. Chem. 491 (2000) 222–233.
[6] A.H.C. Sirk, J.M. Hill, S.K.Y. Kung, V.I. Birss, J. Phys. Chem. B 108 (2004) 689–695.
[7] D.R. Rolison, P.L. Hagans, K.E. Swider, J.W. Long, Langmuir 15 (1999) 774–779.
[8] P.L. Hagans, K.E. Swider, D.R. Rolison, Symposium on Electrode Material and Processes for Energy Conversion and Storage IV (1997) 86-105.
[9] D.R. Rolison, Science 299 (2003) 1698–1701.
[10] J.W. Long, R.M. Stroud, K.E. Swider-Lyons, D.R. Rolison, J. Phys. Chem. B 104 (2000) 9772–9776.
[11] W.E. O'Grady, P.L. Hagans, K.I. Pandya, D.L. Maricle, Langmuir 17 (2001) 3047–3050.
[12] R. Viswanathan, G. Hou, R. Liu, S.R. Bare, F. Modica, G. Mickelson, C.U. Segre, N. Leyarovska, E.S. Smotkin, J. Phys. Chem. B 106 (2002) 3458–3465.
[13] F. Liu, C.-Y. Wang, Electrochim. Acta 50 (2005) 1413–1422.
[14] D. Chakraborty, I. Chorkendorff, T. Johannessen, J. Power Sources 162 (2006) 1010–1022.
[15] A. Havranek, K. Wippermann, J. Electroanal. Chem. 567 (2004) 305–315.
[16] A.G. Hombrados, L. Gonźalez, M.A. Rubio, W. Agila, E. Villanueva, D. Guinea, E. Chinarro, B. Moreno, J.R. Jurado, J. Power Sources 151 (2005) 25–31.
[17] J.S. Lee, K.I. Han, S.O. Park, H.N. Kim, H. Kim, Electrochim. Acta 50 (2004) 807–810.
[18] J.H. Kim, H.I. Lee, S.A. Hong, H.Y. Ha, J. Electrochem. Soc. 153 (2005) A2345–A2351.
[19] S. Sanicharane, A. Bo, B. Sompalli, B. Gurau, E.S. Smotkin, J. Electrochem. Soc. 5 (2002) A554–A557.
[20] J. Jiang, A. Kucernak, J. Electroanal. Chem. 576 (2005) 223–236.
[21] L. Liu, R. Viswanathan, R. Liu, E.S. Smotkin, Electrochem. Solid. State 1 (1998) 123–125.
[22] D. Chakraborty, M.B. Jensen, I. Chorkendorff, T. Johannessen, Proceedings of the 3rd European Fuel Cell Forum Conference CD, Lucerne, Switzerland, 2005, pp. file p. 110.
[23] L. Mädler, H.K. Kammler, R. Mueller, S.E. Pratsinis, J. Aerosol Sci. 33 (2002) 369–389.
[24] J.P. Hansen, J.R. Jensen, H. Livbjerg, T. Johannessen, AICHE J. 47 (2001) 2413–2418.
[25] M.B. Jensen, Anode Optimization for Polymer Electrolyte Fuel Cells—With Flame Spray Pyrolysis Deposited Catalytic Particles, Technical University of Denmark, 2005.
[26] R.R. Diaz-Morales, R. Liu, E. Fachini, G. Chen, C.U. Segre, A. Martinez, C. Cabrera, E.S. Smotkin, J. Electrochem. Soc. 151 (2004) A1314–A1318.
[27] R.M. Stroud, J.W. Long, K.E. Swider-Lyons, D.R. Rolison, Microsc. Microanal. 8 (2002) 50–57.
[28] R.D. Armstrong, M. Henderson, J. Electroanal. Chem. 39 (1972) 81–90.
[29] L. Bai, B.E. Conway, J. Electrochem. Soc. 138 (1991) 2897–2907.
[30] G. Song, A. Atrens, D.S. John, X. Wu, J. Nairn, Corros. Sci. 39 (1997) 1981–2004.
[31] V.S. Bagotzky, Y.B. Vassilev, Electrochim. Acta 12 (1967) 1323–1343.
[32] A. Hamnett, Catal. Today 38 (1997) 445–457.
[33] A. Kabbabi, R. Faure, R. Durand, B. Beden, F. Hahn, J.-M. Leger, C. Lamy, J. Electroanal. Chem. 444 (1998) 41–53.
[34] T. Yajima, H. Uchida, M. Watanabe, J. Phys. Chem. B 108 (2004) 2654–2659.
[35] H.A. Gasteiger, N. Marković, P.N. Ross Jr., E.J. Cairns, J. Phys. Chem. B 97 (1993) 12020–12029.
[36] M.M. Nenad, A.G. Hubert, Ross Jr., X. Jiang, I. Villegas, M.J. Weaver, Electrochim. Acta 40 (1995) 91–98.
[37] C. Krozeniewski, C.L. Childers, J. Phys. Chem. B 102 (1998) 489–492.
[38] M.D. Levi, Z. Lu, D. Aurbach, Solid State Ionics 143 (2001) 309–318.
[39] M.V. Ten Kortenaar, C. Tessont, Z.I. Kolar, H. van der Weijde, J. Electrochem. Soc. 146 (1999) 2146–2155.
[40] G. Wu, Y.-S. Chen, B.-Q. Xu, Electrochem. Commun. (2005) 1237–1243.
[41] M. Mastragostino, A. Missiroli, F. Soavi, J. Electrochem. Soc. 151 (2004) A1919–A1924.

[42] Z. Siroma, T. Sasakura, K. Yasuda, M. Azuma, Y. Miyazaki, J. Electroanal. Chem. 546 (2003) 73–78.
[43] R. Šimpraga, G. Tremiliosi-Filho, S.Y. Qian, B.E. Conway, J. Electroanal. Chem. 424 (1997) 141–151.
[44] S. Wasmus, A. Küver, J. Electroanal. Chem. 461 (1999) 14–31.
[45] G. Stephanopoulos, Chemical Process Control: An Introduction to Theory and Practice, Prentice-Hall of India, New Delhi, 1995, pp. 193–200.
[46] W.L. Holstein, H.D. Rosenfeld, J. Phys. Chem. B 109 (2005) 2176–2186.
[47] J.C. Davies, J. Bonde, A. Logadottir, J.K. N›rskov, I. Chorkendorff, Fuel Cell 05 (2005) 429–435.
[48] S.C. Thomas, X. Ren, S. Gottesfeld, J. Electrochem. Soc. 146 (1999) 4354–4359.
[49] D. Chu, S. Gilman, J. Electrochem. Soc. 143 (1996) 1685–1690.
[50] H.A. Gasteiger, P.N. Ross Jr., E.J. Cairns, Surf. Sci. 293 (1993) 67–80.
[51] V. Radmilovic, H.A. Gasteiger, P.N.J. Ross, J. Catal. 154 (1995) 98–106.
[52] C. Roth, N. Martz, F. Hahn, J.-M. Leger, C. Lamy, H. Fuess, J. Electrochem. Soc. 149 (2002) E433–E439.
[53] S.T. Kuk, A. Wieckowski, J. Power Sources 141 (2004) 1–7.
[54] G. Tremiliosi-Filho, H. Kim, W. Chrzanowski, A. Wieckowski, B. Grzybowska, P. Kulesza, J. Electroanal. Chem. 467 (1999) 143–156.
[55] P. Waszczuk, J. Solla-Gullon, H.-S. Kim, Y.Y. Tong, V. Montiel, A. Aldaz, A. Wieckowski, J. Catal. 203 (2001) 1–6.
[56] D.C. Papageorgopoulos, M.P. de Heer, M. Keijzer, J.A.Z. Pieterse, F.A. de Bruijn, J. Electrochem. Soc. 151 (2004) A763–A768.
[57] M. Watanabe, S. Motoo, J. Electroanal. Chem. 60 (1975) 267–273.
[58] H.A. Gasteiger, N. Marković, P.N. Ross Jr., E.J. Cairns, J. Phys. Chem. 98 (1994) 617–625.
[59] J.C. Davies, B.E. Hayden, D.J. Pegg, Surf. Sci. 467 (2000) 118–130.
[60] J.C. Davies, B.E. Hayden, D.J. Pegg, M.E. Rendall, Surf. Sci. 496 (2002) 110–120.
[61] U.A. Paulus, U. Endruschat, G.J. Feldmeyer, T.J. Schmidt, H. Bonnemann, R.J. Behm, J. Catal. 195 (2000) 383–393.
[62] H.A. Gasteiger, N. Marković, P.N. Ross Jr., E.J. Cairns, J. Electrochem. Soc. 141 (1994) 1795–1803.
[63] Z. Jusys, J. Kaiser, R.J. Behm, Electrochim. Acta 47 (2002) 3693–3706.